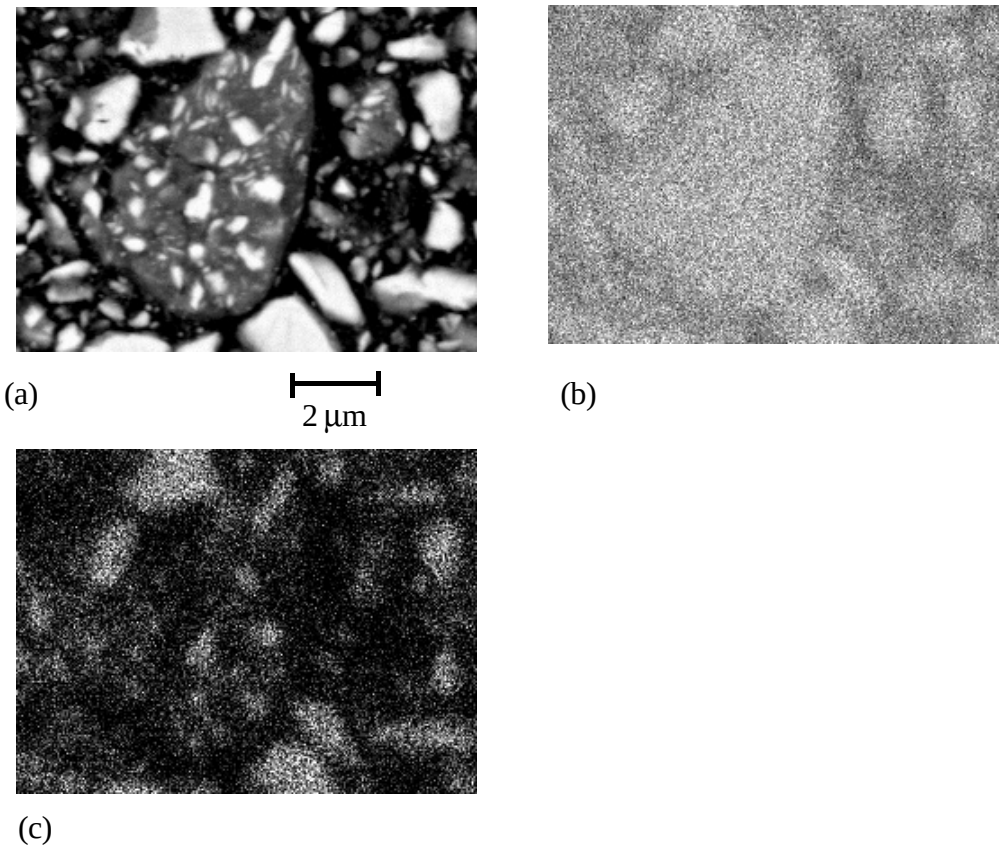

Figure 3.5: (a) SEM image (backscattered electrons) of $SmCo_5$ ball milled with CoO for 16 h, in the weight ratio 1:1, with the corresponding Co (b) and Sm (c) EDX mappings.

3.2.- Structural Characterization:

3.2.1.- The structure evolution and phase transformations induced in ball milled cobalt

The evolution of the x-ray spectra of Cobalt milled alone indicates that it undergoes hexagonal close packed (hcp) – face centered cubic (fcc) allotropic phase transitions during ball milling [5,6]. The particular structural behavior of cobalt during ball milling is analyzed in this section. In order to better control the microstructure evolution during the milling, the ball-to-powder weight ratio was chosen to be relatively low, e.g. 2:1. XRD patterns of Co before milling and after milling for 1 h and 45 h are shown in fig. 3.6 (a). The XRD pattern of the 20 h milled Co, together with the curve generated from the full pattern fitting procedure and the corresponding difference between the calculated and the experimental profiles can be seen in fig. 3.6 (b).

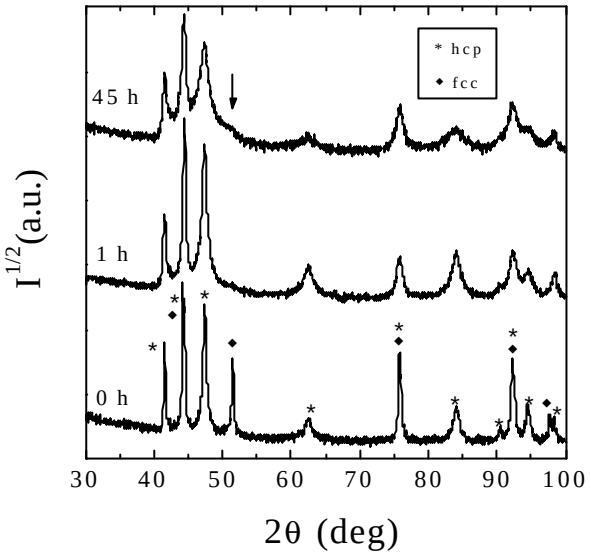

(a)

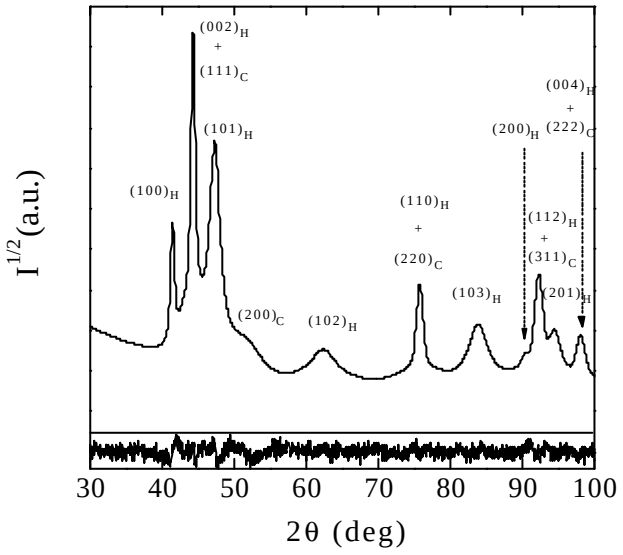

(b)

Figure 3.6: (a) X-ray diffraction patterns of Co before milling and after milling for 1h and 45 h. (b) x-ray diffraction patterns of the 20 h milled Co, together with the curve generated from the full pattern fitting procedure and the corresponding difference between the calculated and the experimental profiles. The symbols ◆ and * in (a) denote the fcc and hcp phases, respectively. Note that the Miller indexes corresponding to each peak have also been indicated in (b) and that H and C subindexes denote hcp and fcc phases, respectively.

The Miller indexes (*hkl*) for the different diffraction peaks are also indicated in fig. 3.6 (b). From fig. 3.6 (a) one can observe that the starting powder is a mixture of hcp and fcc cobalt. However, the amount of fcc rapidly reduces with milling time, as deduced from the decrease in intensity of the fcc peaks, for example of the $(200)_C$ peak (indicated by an arrow in fig. 3.6 (a)), which vanishes almost completely after milling for 1 h. For longer milling times, hcp-Co tends to partially transform back to fcc. This can be seen from the formation of a wide hump after long-term milling at the position corresponding to the $(200)_C$ peak.

X-ray diffraction results were complemented with transmission electron microscopy (TEM) observations, together with selected area electron diffraction (SAED) analyses. The observations were performed after dispersing the powders in ethanol and depositing them on a TEM grid. Electron diffraction has the advantage over x-ray diffraction that it allows structural analysis of a specific area of the sample, for example a set of a few crystallites. TEM observations reveal that after milling for 20 h, the particles are often found to be composed of a large number of grains, which form aggregates of a few μm. The SAED pattern of one of these agglomerates, obtained after dispersing the powders in ethanol for 0.5 min, is shown in fig. 3.7 (a). The SAED pattern corresponds to the aggregate shown in the inset.

A combination of rings and spots, typical of polycrystalline samples, is observed in figure 3.7 (a). Basically, almost all rings can be indexed as hcp-Co, although some traces of fcc-Co can be also identified. The Miller indexes (*hkl*) have been indicated in the figure for each ring (H and C denote hcp and fcc phases, respectively). These results are in good agreement with XRD results, since both reveal that after long-term milling a certain amount of Co is in the fcc phase [5,6].

When the particles are further ultrasonically dispersed in ethanol (for 5 min), the majority of clusters disaggregate and the mean grain size is found to be of about 25 nm (see fig. 3.7 (b)).

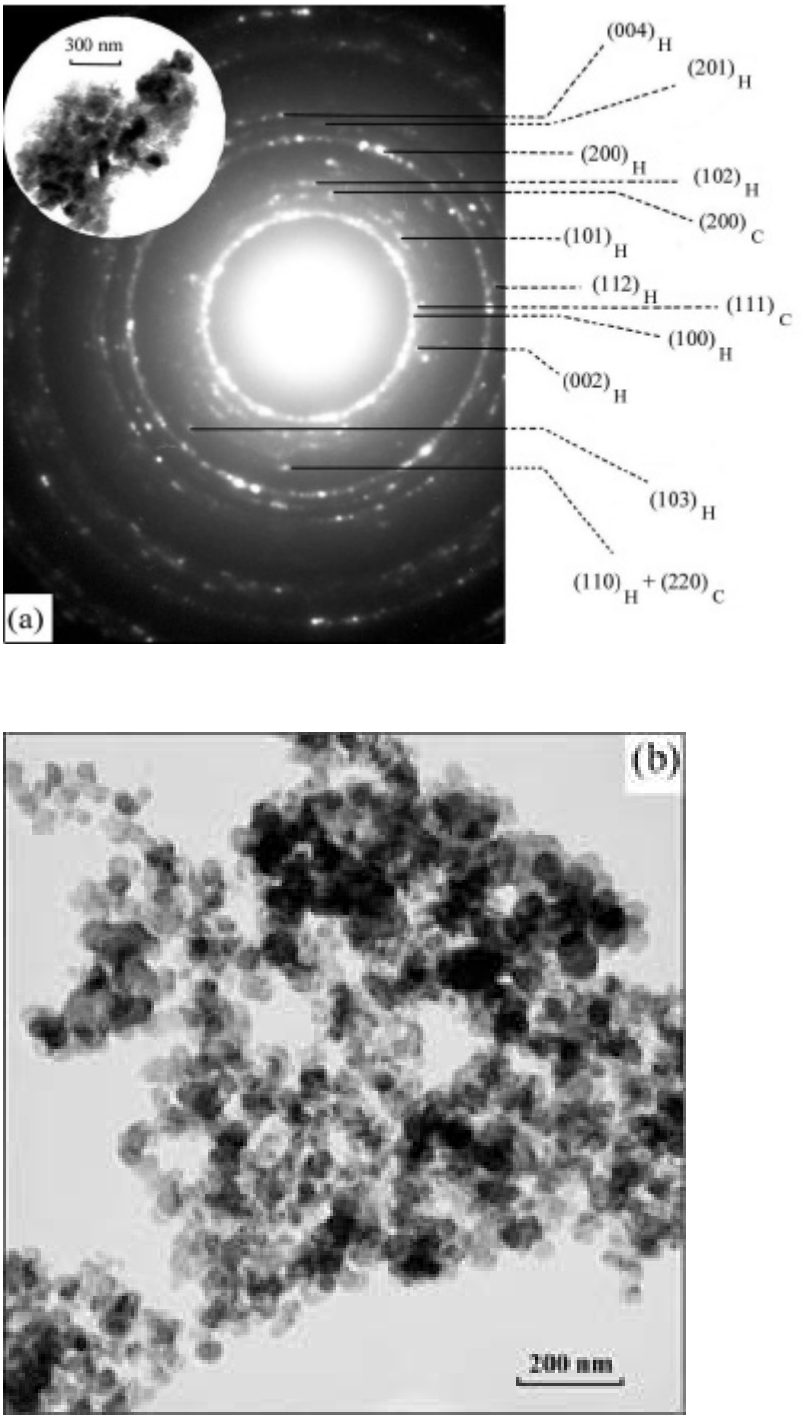

Figure 3.7: (a) Selected area electron diffraction pattern corresponding to the particle imaged in the inset, which is an aggregate of Co crystallites, formed during milling for 20 h at 500 rpm. For this observation, the as-milled powders were previously ultrasonically dispersed in ethanol during 0.5 min. (b) Transmission electron diffraction image of 20 h ball milled Co particles after dispersing in ethanol during 5 min.

The weight percentages of hcp and fcc phases, evaluated from a full-pattern fitting procedure of XRD data using MAUD program (Rietveld method) are shown in fig. 3.8 as a function of milling time. The fcc content in the unmilled material is of about 32 % (weight percent). As the milling time increases, the fcc percentage is found to steeply decrease. A maximum hcp percentage (of around 94 %) is obtained after 1 h of milling. During the next hours, the fcc amount seems to gradually increase again, reaching a value of about 15 % after milling for 20 h. For longer times the fcc content is found to level off, indicating that, for a fixed milling intensity, the increase of milling time does not bring about further transformation from hcp to fcc cobalt.

The transformation from fcc-Co to hcp-Co induced by cold-work is a well-known effect [9]. Basically, since fcc is a high-temperature phase (it is only stable for $T > 695$ K) it turns out to be essentially metastable at room temperature. Thus, the amount of fcc present in the unmilled Co powders, still remaining from the gas atomisation processing of the as-bought particles, tends to transform to hcp during the first stages of milling. This transformation proceeds via formation and motion of Shockley partial dislocations, which enclose deformation-type stacking faulted regions [10].

The reverse transformation, i.e. from hcp to fcc, induced after long-term milling, is probably also related to accumulation of a large amount of stacking faults. The formation of fcc-Co by ball milling was first observed by Cardellini and Mazzone in 1993 when pure hcp Co powders were ball milled in hardened steel vials and balls [11]. They explained the fcc formation in terms of the Fe contamination resulting from the milling process, since, according to the phase diagram, small additions of Fe into Co can shift the hcp to fcc transition temperature, T_t, from 695 K to approximately 0 K [12]. Similar results were also obtained by Huang and co-workers [13]. However, they reported that a certain amount of fcc-Co could also be obtained after milling in agate vials and balls, thus pointing out that the introduction of structural defects could play some role in the transformation [14]. It is noteworthy that, when milling in agate, Huang and co-workers failed to obtain pure fcc phase, even after long-term milling, which might suggest that Fe-contamination may play an important role in the formation of fcc-Co phase by ball milling.

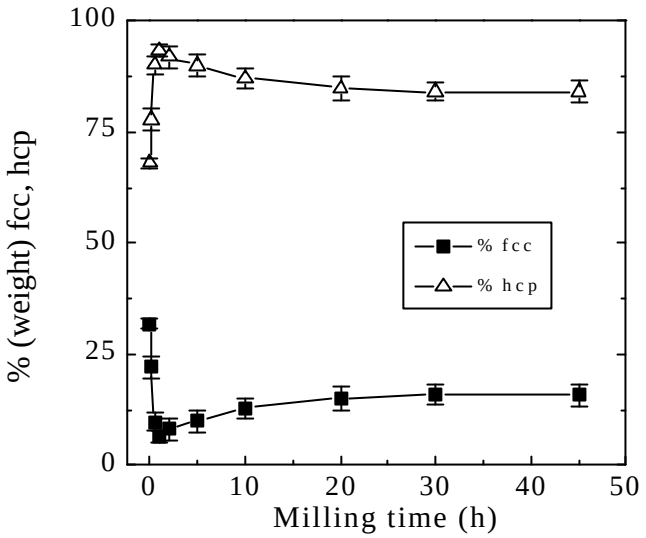

Figure 3.8: Milling time dependences of the hcp (--△--) and fcc (--■--) weight percentages. Note that the lines are a guide to the eye.

Several features of the XRD patterns are worth mentioning. First, according to the powder diffraction files database [15], the $(101)_H$ peak should be the most intense. Thus, the higher intensity obtained in the $(002)_H$ peak (see fig. 3.6) indicates that some texture is present in the sample. Note that, due to the overlap between the $(002)_H$ and the $(111)_C$ peaks, this preferred orientation is most unambiguously apparent in the 1 h milled Co pattern, where the fcc contribution is almost negligible. Texture probably originates from the platelet shape of the particles, described in section 3.1, which makes them arrange anisotropically when they are spread on the XRD holder, i.e. with the basal planes of the platelets parallel to the holder surface.

Moreover, as the milling time increases the XRD peaks progressively broaden. This is because of the milling-induced crystallite size refinement and the increase of microstrains. The milling time evolution of the average crystallite size, $\langle D \rangle_H$, and microstrain, $\langle \varepsilon^2 \rangle^{1/2}_H$, for the hcp phase, is shown in fig. 3.9. The small amount of fcc present for intermediate milling times makes it impossible to plot the temporal evolution of crystallite size and microstrain for this phase. However, $\langle D \rangle_C$ and $\langle \varepsilon^2 \rangle^{1/2}_C$ can be determined either for very short or long enough milling times. Thus, in the unmilled Co, the crystallite sizes are of about 67 and 80 nm for the hcp and fcc phases, respectively. In both phases, $\langle D \rangle$ is found to significantly reduce as the milling time increases, reaching, for the hcp phase, a value of

$<D>_H$ = 16 nm after milling for 20 h (see fig. 3.9). This value is slightly lower than the mean crystallite size observed by TEM (see fig. 3.7 (b)). This can be due to the disordered character of the grain boundaries, which decreases the coherence length and thus the crystallite size, as determined by XRD. For longer milling times, $<D>_H$ remains almost constant. For the fcc phase $<D>_C$ is found to be less than 4 nm after milling for 45 h, indicating that after such a long-term milling, as will be discussed later, fcc-Co should be considered as an accumulation of stacking faults in the hcp structure [5].

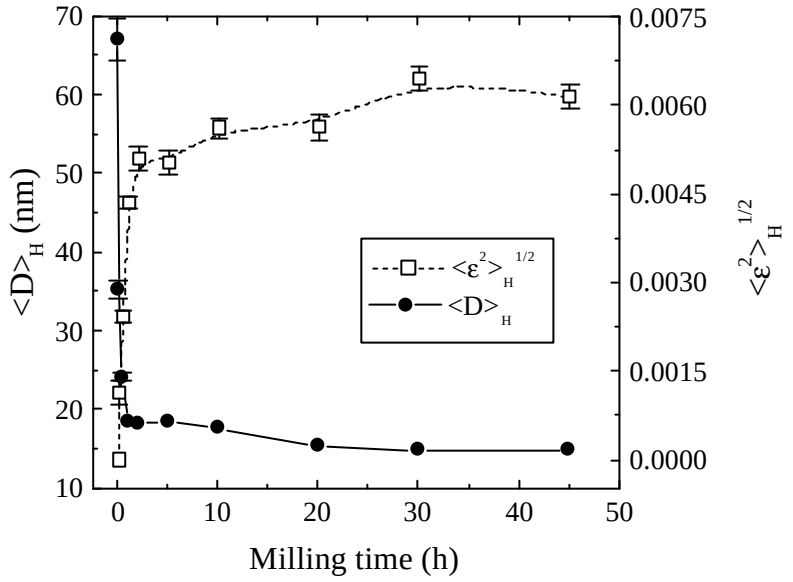

Figure 3.9: Milling time dependences of the mean crystallite size, $<D>_H$, (—●—) (evaluated from the XRD peaks not affected by the extra-broadening due to stacking faults), and the microstrains, $<\varepsilon^2>^{1/2}_H$, (--□--), for the hcp-Co phase. Note that some error bars in $<D>_H$ are included within the size of the symbols and the lines are a guide to the eye.

Conversely, $<\varepsilon^2>^{1/2}_H$ increases with the milling time. In the starting material, $<\varepsilon^2>^{1/2}$ is found to be approximately zero in both hcp and fcc phases. However, for hcp, $<\varepsilon^2>^{1/2}_H$ increases steeply during the first 2 h of milling and reaches a maximum value of about 0.0064 after long-term milling. Similar values of $<\varepsilon^2>^{1/2}_C$ are found for fcc-Co after long-term milling. The high values of $<\varepsilon^2>^{1/2}_H$ and $<\varepsilon^2>^{1/2}_C$ are probably due to the high density of dislocations and grain boundaries developed during the milling process [16].

Figure 3.6 (b) also shows that the hcp peaks satisfying the condition $h - k = 3n + 1$ (where n is an integer) and $l = 0$ are extra-broadened with respect to the other peaks. This is a consequence of the existence of stacking faults [17]. As for $<D>$ and $<\varepsilon^2>^{1/2}$, the stacking fault probabilities in the hcp phase can be determined for all milling times, while for the fcc

phase, the obtained probabilities are only reliable during the first and last stages of milling. Actually two different types of stacking faults, deformation and twin faults, are created in the hcp and fcc phases during the milling. The stacking faults (deformation and twin) probabilities are determined following Warren's formulae, of which a brief description is given in appendix I. Fig. 3.10 shows the probability of finding a deformation-type, α_H, and a twin-type, β_H, stacking fault in hcp-Co, between any two consecutive {001} compacted layers, as a function of milling time.

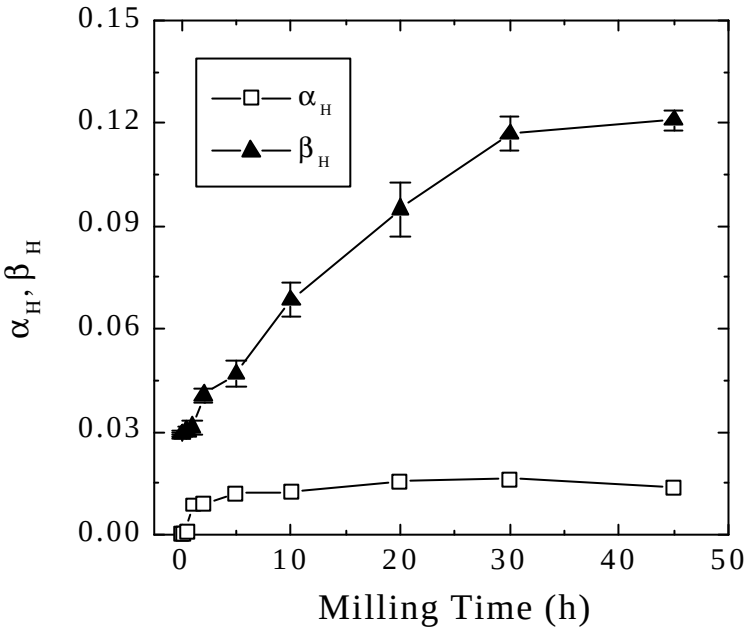

Figure 3.10: Milling time evolution of the deformation-type stacking faults probability, α_H (--□--), and the twin-type stacking fault probability, β_H (--▲--), for the hcp phase. The lines are a guide to the eye. Note that for deformation faults, the error bars are smaller than the symbols.

According to Warren's formulae, $1/\alpha$ and $1/\beta$ indicate the average number of layers between two deformation and twin faults, respectively [17]. In line with the theory of dislocations, deformation faults originate from partial slip between two consecutive compact layers, while twin faults result from twins, i.e. changes in the orientation of a portion of the crystal in such a way that one region takes up an orientation that is the mirror image of the parent crystal [18]. Both types of faults bring about a change of the stacking sequence, from the hexagonal …ABABABAB… to a faulted …AB**ABCA**CA… (for deformation faults) and …AB**ABC**BCB…(for twin faults). Here, the letters A, B and C represent the conventional close-packed planes, which in hcp-Co are the $\{001\}_H$, while the bold letters indicate local fcc packing, along the $\{111\}_C$ direction, generated by the stacking sequence alteration. It should

be noted that, already before the milling, there are a certain number of stacking faults in the particles. This is probably due to the gas-atomization method used to produce the as-bought powders, although usually hcp-Co is intrinsically faulted. As seen in fig. 3.10, both α_H and β_H increase with milling time, tending to level off after long-term milling. However, twin faults are found to predominate over deformation faults for all milling times. This is probably due to the limited number of slip systems in hcp crystals [8,19]. Actually, it is known that in hcp crystals the yield stress for twinning becomes lower than the yield stress for slip under conditions or rapid rate of loading [19]. Therefore, during ball milling the main mechanism of plastic deformation in the hcp crystals is the creation of twins. The high values of α_H and β_H suggest that after long-term milling the stacking faults are so abundant that the material is close to a random stacking sequence [5,6].

It could be argued that the crystallite size reduction can be the main reason for the milling-induced transformation from hcp to fcc. Numerous studies indicate that, due to surface energy considerations, T_t can be significantly lowered when grain size is reduced to a few nanometers, thus stabilizing fcc [20]. In fact, fcc-Co particles, with mean size of about 10 nm, have been synthesized by means of magnetron sputtering and chemical methods and found to be relatively stable at room temperature [21]. However, this possibility has to be also ruled out when the milling time dependences of $<D>_H$ and fcc percentages are compared. As can be seen in fig. 3.9 the major $<D>_H$ change occurs during the first hour of milling and it decreases only slightly afterwards. On the contrary, the formation of fcc starts after milling for 1 h, indicating that both effects are not necessarily closely related to each other. Another possible hypothesis for the fcc formation could be the local temperature rise, ΔT, that takes place during the milling due to the impacts between powders and balls. However, although several reports give estimations of ΔT to be between 30 and 300 K, depending on the mill type, it is generally accepted that, for a fixed milling intensity, the local temperature rise should be essentially the same as the milling proceeds [22]. Therefore, the fact that fcc is first transformed to hcp, in the beginning, and then converted back to fcc for longer milling times also excludes that the local temperature rise is responsible for the hcp to fcc transformation.

Conversely, our results indicate that the formation of fcc is closely related to the amount of stacking faults accumulated during the milling [5,6]. In fact, it is energetically favorable that large amounts of stacking faults are generated during the milling, since the energy stored during a ball milling process of pure metals can be easily higher than 10^3 J· mole^{-1} [23], while the stacking fault energy for Co has been estimated to be of the order of 10^{-3} J· mole^{-1} [24,25]. From figures 3.8 and 3.10 it can be seen that, after 1 h of milling, both β_H and the fcc content increase with the milling time, tending to level off after 30 h of milling. Thus, it can be argued that stacking faults formed during the milling in the hcp structure act like embryos for the nucleation of small fcc crystallites. The nucleation of thin fcc lamellas,

of a few atoms, in the hcp phase tend, by coalescence, to progressively enlarge the regions with fcc structure in the overall material. Moreover, taking into account that it has been theoretically shown that both fcc and hcp phases can be described as resulting from different ordering mechanisms of a common disordered polytype [25,26], it is very appropriate to consider the transformation from hcp to fcc in terms of stacking faults accumulation.

It has been shown in figs. 3.8, 3.9 and 3.10 that many structural parameters in the hcp phase tend to become rather constant after milling for several hours. For instance, the overall stacking fault probability is found to increase only slightly after milling for 20 h. Moreover, the fcc content in the as-milled powders also becomes virtually unchanged after 20 h (see fig. 3.8). This leads to the question of whether an increase of the milling intensity may have any influence on the formation of fcc-Co. To study this possibility, table 3.1 shows the effect of varying the ball-to-powder weight ratio, fixing the milling time to 45 h (i.e. in the steady state). As expected, both a_H and b_H increase with the ball-to-powder ratio and, consistently, an enhancement of the fcc percentage is also observed. Moreover, the slight increase of $\langle D \rangle_C$ with the milling energy (see table 3.1) confirms that when the fault probability becomes high enough, stacking faults may somehow coalesce, thus enlarging the extent of the regions with fcc stacking sequence in the overall material. However, $\langle D \rangle_C$ is very small (i.e. only a few lattice constants), thus it can hardly be designated as an actual crystallite size, especially in such a disordered material, i.e. with large amounts of stacking faults. Consequently, we can consider the material, especially for the highest milling energies, to be close to a random sequence of close-packed stacking planes where *locally* they tend to be more hcp or fcc-like [6].

	$\langle D \rangle_H$ (nm) (± 0.3)	$\langle e^2 \rangle^{1/2}_H$ (± 0.1 x 10^{-3})	a_H (±0.002)	b_H (±0.003)	$\langle D \rangle_C$ (nm) (± 0.3)	% fcc (weight) (± 1)
45 h, 2:1	14.9	6.1 x 10^{-3}	0.013	0.121	2.3	16
45 h, 5:1	9.4	7.3 x 10^{-3}	0.036	0.147	2.7	27
45 h, 10:1	8.7	7.6 x 10^{-3}	0.058	0.169	3.2	33
45 h, 20:1	6.6	7.9 x 10^{-3}	0.074	0.178	3.6	41

Table 3.1: Microstructural parameters of Co powders milled for 45 h, at 500 rpm, in different ball-to-powder weight ratios: 2:1, 5:1, 10:1 and 20:1.